22nd Applied Aerodynamics Conference and Exhibit
16 - 19 August 2004, Providence, Rhode Island

AIAA 2004-5377

22nd AIAA Applied Aerodynamic Conference and Exhibit
August 16–19, 2004/Providence, Rohde Island

Time-Domain Aeroelastic Simulation by a Coupled Euler and Integral Boundary-Layer Method

Shuchi Yang*, Zhichao Zhang †, Feng Liu‡, Shijun Luo§
Department of Mechanical and Aerospace Engineering
University of California, Irvine, CA 92697-3975

Her-Mann Tsai¶
Temasek Laboratories
National University of Singapore
Kent Ridge Crescent, Singapore 119260

David M. Schuster‖
Aeroelasticity Branch
NASA Langley Research Center, Hampton, VA 23681

An interactive boundary-layer method that solves the unsteady Euler equations coupled with Green's lag entrainment integral boundary-layer equations is presented for time domain aeroelastic computation. The three-dimensional unsteady Euler equations are solved on stationary body-fitted curvilinear grids. Unsteady boundary conditions on moving surfaces in an aeroelastic problem are accounted for by using approximate small-perturbation method without moving the computational grid. A semi-inverse method is used to couple the Euler and the boundary-layer solutions in order to compute flows with strong inviscid and viscous interactions. The method is tested on standard steady transonic flow computations for the NACA0012 and RAE2822 airfoils and computations of three-dimensional steady and unsteady flows of the LANN Wing. Comparisons with Navier-Stokes results and available experimental data show that the interactive-boundary-layer method provides significant improvement over inviscid calculations by the Euler equations alone. The proposed method is used to predict the flutter boundary for the Isogai wing test case through time domain simulations. The interactive boundary-layer result agrees with that by a Navier-Stokes solver and indicates fundamental differences between the viscous and inviscid solutions in the transonic range.

I. Introduction

Flutter is one of the most critical technical problems for the aircraft and it effects the reliability, cost and safety of the vehicle. It is a catastrophic aeroelastic phenomenon that must be avoided at all costs.[1] In order to understand this complex phenomenon, we need to model both fluid and structure by coupling the fluid dynamics solver and the structural dynamics solver. During the coupling process, we need to solve the structure and fluid governing equations at the same time (fully coupled) or alternatively (loosely coupled) at each time step. After each step the aerodynamic forces and structured deformation need to be transfered

*Post-Doctoral Researcher, Member AIAA.
†Graduate student, Member AIAA.
‡Professor. Associate Fellow AIAA.
§Researcher.
¶Principal Research Scientist. Member AIAA.
‖Senior Research Engineer. Associate Fellow AIAA.

between the two solvers. The grid for the flow solver needs to be deformed or regenerated according to the structural deformation at each time step.

The selection of the governing equation for flow solver greatly affects the computational time. An Euler solver captures all the flow characteristic of the transonic flow except viscous effects. A flow solver with Navier-Stokes equations includes the effect of the viscosity but is time consuming. In order to take account for the viscous effect and reduce the computational cost, a boundary layer coupling method can be used. Boundary layer coupling method provides a good balance between completeness of the flow model and computational efficiency.

Similar to the authors' another paper,[2] the integral boundary layer method is used and coupled with the Euler solver following J. E. Cater's "semi-inverse" coupling scheme. First, a guessed boundary layer thickness, together with the velocity and density near the wall from Euler solver is used to compute the perturbation mass flow. Second, the transpiration velocity is used in the Euler solver to simulate the perturbation mass flow to solve the flow field. Third, the velocity and density near the wall are extracted from the Euler flow field and used to update the guess of the boundary thickness distribution. The process is repeated until converges. As mentioned above the blowing velocity (transpiration velocity) is used to take account the viscous effect in Euler solver, which is implemented together with the simplified boundary condition in a uniform way for the unsteady and aeroelastic computations.

The formulation of the proposed approximate boundary conditions and boundary layer method are presented first. They are implemented in a three-dimensional body-fitted grid code, PARCAE(PARallel Computation of AeroElasticity)[3–5] developed at UCI. Then the boundary-layer coupling method is validated for steady cases. Later the method is used to compute the unsteady pitching flow field around the LANN Wing. The computational results are compared with the experimental data. At last, these methods are used to compute the flutter boundary of Isogai wing and compare the result with that from Euler solver and known Navier-Stokes solution.

II. Governing Equations

The two-dimensional unsteady Euler equations in conservative integral form over a fixed control volume V enclosed by the surface S in the Cartesian coordinate system (x, y) are

$$\frac{\partial}{\partial t}\int_V \mathbf{W} dV + \int_S \mathbf{G}\cdot\mathbf{n} dS = 0 \tag{1}$$

where

$$\mathbf{W} = \begin{bmatrix} \rho \\ \rho u \\ \rho v \\ \rho E \end{bmatrix} \tag{2}$$

$$\mathbf{G} = \begin{bmatrix} \rho\mathbf{q} \\ \rho u\mathbf{q} + p\mathbf{e}_x \\ \rho v\mathbf{q} + p\mathbf{e}_y \\ \rho E\mathbf{q} + p(u\mathbf{e}_x + v\mathbf{e}_y) \end{bmatrix} \tag{3}$$

$$\mathbf{q} = u\mathbf{e}_x + v\mathbf{e}_y \tag{4}$$

$$E = \frac{1}{\gamma - 1}\frac{p}{\rho} + \frac{1}{2}(u^2 + v^2) \tag{5}$$

$$H = E + \frac{p}{\rho} \tag{6}$$

Following the procedure by Liu and Jameson,[6] a cell-centered finite-volume method and a Runge-Kutta multi-step scheme are used for the space discretization and time marching respectively. Scalar and matrix artificial dissipation schemes are used to prevent oscillations near stagnation points and shock waves. In order to accelerate the computation, local time steps and multi-grid are implemented. For unsteady cases, dual time-stepping is used to do the fully implicit time marching.[7]

III. Simplified Boundary Conditions

For an airfoil with small deformation or rotation, the original airfoil and the new position are considered as shown in Fig. 1. An arbitrary point $P_0(x_0,y_0)$ on the original airfoil moves to a new position P(x,y). For unsteady computation, the velocity boundary condition at P should be

$$\mathbf{q} \cdot \mathbf{n} = \mathbf{q}_b \cdot \mathbf{n} \tag{7}$$

where $\mathbf{q}_b$ is the velocity of the airfoil for unsteady cases and $\mathbf{n}$ is the unit normal vector at P. Using Taylor expansion, the flow variables at P can be represented by those at P_0:

$$\mathbf{q}(x,y) = \mathbf{q}(x_0,y_0) + \frac{\partial \mathbf{q}}{\partial x}(x_0,y_0)(x-x_0) + \frac{\partial \mathbf{q}}{\partial y}(x_0,y_0)(y-y_0) + O(\Delta r^2) \tag{8}$$

If the deformation of the airfoil is small, which means that $\Delta r = \sqrt{(x-x_0)^2+(y-y_0)^2} \ll$ c (airfoil chord), we have

$$\mathbf{q}(x,y) = \mathbf{q}(x_0,y_0) + O(\Delta r) \tag{9}$$

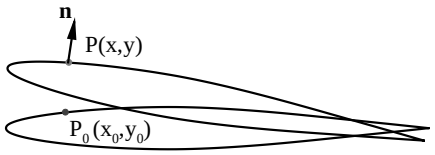

Figure 1. Description of the movement of the airfoil.

Then equation (7) can be written as

$$\mathbf{q}(x_0,y_0) \cdot \mathbf{n} = \mathbf{q}_b \cdot \mathbf{n} \tag{10}$$

We can transform the above equation to a local grid coordinate system (ξ,η), and use the contravariant velocity (U,V). The relation between (U,V) and (u,v) is

$$\begin{aligned} u &= x_\xi U + x_\eta V \\ v &= y_\xi U + y_\eta V \end{aligned} \tag{11}$$

Substituting equation (11) to equation (10), we get the following approximate wall boundary condition.

$$V = -\frac{U(x_\xi n_x + y_\xi n_y) - (u_b n_x + v_b n_y)}{(x_\eta n_x + y_\eta n_y)} \tag{12}$$

Notice in the above equation, although the flow velocities are evaluated at the stationary position P_0, the normal vector $\mathbf{n}$ is evaluated at the actual point P, which changes with time. In addition, u_b and v_b, the local body velocity components, are obtained from the actual unsteady motion of the airfoil.

In the same way, we can deal with the normal momentum equation, which is used to compute the pressure on the wall.

$$\mathbf{n} \cdot [\frac{\partial \mathbf{q}}{\partial t} + (\mathbf{q} \cdot \nabla)\mathbf{q}] = \mathbf{n} \cdot (-\frac{\nabla p}{\rho}) \tag{13}$$

Since we are using first-order approximation in this paper, we use the zero-th-order extrapolation to get the pressure on the wall which is directly extrapolated from the first interior grid cells for the simplified boundary condition computations.

IV. Integral Boundary Layer Method

On consideration of computational cost as well as uncertainties of turbulence modeling involved in the Reynolds-Averaged Navier-Stokes equations method, we use an integral boundary-layer method to account for the viscous effect. The classical boundary-layer calculation is to solve the boundary-layer thickness using the boundary-layer edge pressure gradient obtained from the outer inviscid flow solver. However, it is well known that this so-called direct method of boundary-layer calculation breaks down for flows involving strong inviscid-viscous interactions, especially when separation exists. Thus we couple the inverse boundary-layer calculation with the outer inviscid flow solution. In an inverse boundary-layer calculation, on the other hand, the edge pressure or velocity is solved from a given distribution of boundary-layer displacement thickness. More conveniently, following Cater[8] , we introduce the perturbation mass flow parameter $\overline{m} = \rho_e U_e \delta^*$. For a given distribution of $\overline{m}$ along the wall, we solve for the boundary-layer edge velocity U_e.

By definition, $\delta^* = H\theta$, so expanding $\frac{d\overline{m}}{ds} = \frac{d(\rho_e U_e H\theta)}{ds}$ we get:

$$\frac{1}{\overline{m}}\frac{d\overline{m}}{ds} = \frac{1}{H}\frac{dH}{ds} + \frac{1}{\theta}\frac{d\theta}{ds} + (1-M_e^2)\frac{1}{U_e}\frac{dU_e}{ds} \tag{14}$$

where δ and θ are the boundary-layer displacement and momentum thicknesses; ρ_e, U_e and M_e are local air density, velocity, and Mach number at the boundary-layer edge, respectively; s is the streamwise coordinate along the airfoil wall or wake; H is the boundary-layer shape factor.

Considering the correlation between the shape factor H and the kinematic shape factor $\overline{H}$, i.e. $H = R_1(\overline{H}+1) - 1$, we have

$$\frac{dH}{ds} = R_1\frac{d\overline{H}}{ds} + (H+1)\frac{R_3}{U_e}\frac{dU_e}{ds} \tag{15}$$

Thus Eqn. (14) becomes:

$$\frac{H\theta}{\overline{m}}\frac{d\overline{m}}{ds} = H\frac{d\theta}{ds} + R_1\theta\frac{d\overline{H}}{ds} + [(H+1)R_3 + H(1-M_e^2)]\frac{\theta}{U_e}\frac{dU_e}{ds} \tag{16}$$

Here, R_1, R_2, and R_3 are three parameters defined for convenience which are related to the ratio of specific heats γ, temperature recovery factor r, and the local boundary-layer edge Mach number M_e :

$$\begin{aligned} R_1 &= 1 + \frac{\gamma-1}{2} r M_e^2 \\ R_2 &= 1 + \frac{\gamma-1}{2} M_e^2 \\ R_3 &= \frac{(\gamma-1) r M_e^2 R_2}{R_1} \end{aligned}$$

For a turbulent boundary-layer, Head[9] introduced the entrainment coefficient C_E, which stands for the rate at which fluid from the outer inviscid flow enters the boundary-layer through the boundary-layer edge. From the continuity equation, we can easily derive

$$C_E = \frac{1}{\rho_e U_e}\frac{d(\rho_e U_e H_1 \theta)}{ds} \tag{17}$$

where H_1 is Head's shape factor. Again, expanding the derivative we get:

$$C_E = H_1\frac{d\theta}{ds} + H_1(1-M_e^2)\frac{\theta}{U_e}\frac{dU_e}{ds} + \theta\frac{dH_1}{d\overline{H}}\frac{d\overline{H}}{ds} \tag{18}$$

In addition, we have the integral momentum equation for the compressible boundary-layer:

$$\frac{C_f}{2} = \frac{d\theta}{ds} + (H+2-M_e^2)\frac{\theta}{U_e}\frac{dU_e}{ds} \tag{19}$$

Thus we obtain a linear system of equations (16), (18), and (19) about three unknown derivatives : $\frac{d\theta}{ds}$,$\frac{dU_e}{ds}$, and $\frac{d\overline{H}}{ds}$. Solving it, we have now a system of three first-order ordinary differential equations about three boundary-layer parameters: θ, U_e, and $\overline{H}$.

In addition, we employ Green's lag equation[10] to account for the history effects in a non-equilibrium turbulent boundary-layer:

$$\theta\frac{dC_E}{ds} = \overline{F}\left\{\frac{2.8}{H+H_1}\left[(C_\tau)^{0.5}_{EQ0} - \lambda(C_\tau)^{0.5}\right] - \left[1+0.075M_e^2\frac{R_1}{1+0.1M_e^2}\right]\frac{\theta}{U_e}\frac{dU_e}{ds} + \left(\frac{\theta}{U_e}\frac{dU_e}{ds}\right)_{EQ}\right\} \quad (20)$$

Here, C_τ is the shear stress coefficient, λ is a parameter to account for secondary effects, $\overline{F}$ is another parameter to be defined in Ref. 2. The subscript EQ denotes quantities evaluated under equilibrium conditions where the shape factor and the entrainment coefficient are invariant, while $EQ0$ denotes quantities evaluated under equilibrium flow free of secondary effects.

Therefore, totally we have a system of four first-order ordinary differential equations for the four unknown boundary-layer parameters . Given a distribution of $\overline{m}$ along the wall plus the initial values at a starting point such as a fixed transition point, we can integrate the four ordinary differential equations using Runge-Kutta method and solve for the four unknown boundary-layer parameters: θ, U_e, $\overline{H}$, and C_E. As for correlations of various parameters appeared in the four equations (i.e., C_f, F, H_1, C_τ, $(\frac{\theta}{U_e}\frac{dU_e}{ds})_{EQ}$, and $(C_\tau)^{0.5}_{EQ0}$, etc.), we follow those in Green's paper[10] . Details could be found from paper.[2]

V. Inviscid-Viscous Coupling Procedure

Given the boundary-layer edge properties obtained from the outer inviscid solver, we can use Thwaites' method[11] to calculate the laminar part of the boundary-layer starting from the stagnation point. Transition is either specified or determined using Michel's formula[12] : $Re_\theta > 1.174(1+22400/Re_s)Re_s^{0.46}$. For the turbulent part, the boundary-layer calculation needs to be coupled with the outer Equivalent Inviscid Flow(EIF) calculation. We employ Carter's "semi-inverse" coupling scheme[13] . We first guess a distribution of the boundary-layer displacement thickness δ^*. Using ρ_e and U_e from a preliminary inviscid calculation, we obtain a guessed perturbation mass flow parameter $\overline{m} = \rho_e U_e \delta^*$. An inverse boundary-layer calculation following the last section gives us a viscous version of the boundary-layer edge velocity U_{ev}. Also from $\overline{m}$, we can derive the wall and wake boundary-conditions for the EIF calculation. Solving the Euler equations with these boundary-conditions for the outer EIF, we have an inviscid version of boundary-layer edge velocity U_{ei}. Then we can use Carter's relaxation scheme[13] to get an updated guess of the boundary-layer thickness:

$$\frac{\delta^*_{new}}{\delta^*_{old}} = 1+\omega\left(\frac{U_{ev}}{U_{ei}} - 1\right) \quad (21)$$

Here, ω is an under-relaxation factor. Convergence is judged from the difference between the two boundary-layer edge velocities U_{ev} and U_{ei} . Two orders-of-magnitude drop of the difference between these two velocities over the inviscid one is enough for most of cases.

As we solve the Euler equations for the outer EIF, on the airfoil wall, we need four boundary-conditions from the matching requirements of the EIF with the viscous flow for a 2D problem. However, as Sockol and Johnston[14] proved, if we use the surface normal blowing velocity derived from the continuity equation as a boundary condition, then other matching requirements such as the normal flux of stream wise momentum and total enthalpy will automatically be satisfied. Considering first-order boundary-layer approximation, we can simply calculate the surface values of density, stream wise velocity, and total enthalpy via linear extrapolation from the adjacent grid to the wall. Therefore the only change in solving the EIF is that we need to add a blowing velocity in Eqn.(12). The blowing velocity can be obtained from mass conservation:

$$V_n = \frac{1}{\rho_e}\frac{d}{ds}(\rho_e U_e \delta^*) = \frac{1}{\rho_e}\frac{d}{ds}(\overline{m}) \quad (22)$$

It is known that the Kutta condition is automatically satisfied in Euler calculations. So in the wake, unlike the boundary-layer coupling with a potential code, we do not need to bother with jump conditions. We simply treat the wake as two boundary-layers developed on both sides of the dividing streamline of the wake. Currently we assume this dividing streamline is the extension of the airfoil mean chord rather than calculating it accurately.

VI. Results and Discussions

A. Validation of the Boundary Layer Method

In order to validate the proposed interactive boundary-layer method, we first test it for two steady cases. One is for the NACA0012 airfoil at $M_\infty = 0.775$ and $\alpha = 2.05°$ and the Reynolds number based on the chord: Re_c=1×10^7. The other for the supercritical airfoil RAE2822 at $M_\infty = 0.725$ and $\alpha_{exp} = 2.92°$ (the corrected value $\alpha_c = 2.54°$ is used in our calculation) and the Reynolds number based on the chord: Re_c=6.5×10^6. Figure 2 shows the comparisons of computed pressure distributions with experimental data[15,16] for the two cases, respectively. The results with the boundary layer effect considered agree with experimental data very well. The shock position is shifted forward and the strength weakened compared to the pure inviscid solution.

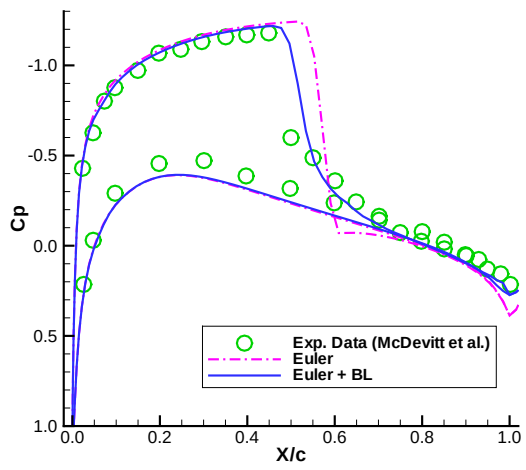

(a) NACA 0012 airfoil at $M_\infty = 0.775$, $\alpha = 2.05^o, Re_c = 10^7$

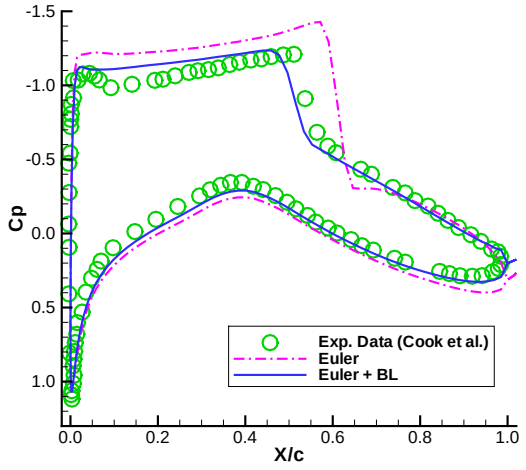

(b) RAE2822 airfoil at $M_\infty = 0.725$, $\alpha = 2.54^o$, $Re_c = 6.5 \times 10^6$

Figure 2. Comparison of calculated and experimental pressure coefficient.

B. LANN Wing Unsteady Computation

Three-dimensional flows over the LANN Wing[17] are simulated by using the present coupled Euler and boundary-layer method. The sections of the LANN Wing are supercritical airfoils. The wing is twisted from 2.6 degree at the root section and -2.0 degree at the tip section. The aspect ratio of the wing is 7.92. The taper ratio is 0.4 and the quarter-chord swept angle is 25 degrees. In order to couple the boundary-layer equations, C-H grids are used for the Euler, Euler-BL and Navier-Stokes computations. Totally $193\times49\times49$ grid points are used for the Euler and Euler-BL computations and $193\times65\times49$ grids points are used for the Navier-Stokes computations. The Baldwin-Lomax turbulence model is used for the Navier-Stokes computations.

Prior to the unsteady computation, the steady flowfield is computed and used as the initial flowfield for the unsteady computation. The Mach number M_∞ is 0.822, and the angle of attack α is 0.6°. The comparisons of pressure distributions are shown in Fig.3. The strength and position of the shock waves predicted by the Euler solver with boundary layer correction are more accurate than those by the Euler solver. The results by the inviscid-viscid coupled solution are close to those by the Navier-Stokes solver. Both viscous solutions improve pressure distribution near the trailing edge on the lower surface of the wing.

Next, an unsteady case is used to test the accuracy of the proposed method. The wing oscillates around an unswept axis at 62.1% of the root chord in a pitch motion as

$$\alpha(t) = \alpha_m + \alpha_0 \sin \omega t \tag{23}$$

In this case, the mean angle of attack α_m=0.6°, the pitching amplitude α_m=0.5°, and the reduced frequency $\kappa = \frac{\omega c_r}{2U_\infty}$=0.102, where c_r is the chord of the root section. The Reynolds number based on the root chord: Re=7.3×10^6. The Mach number M_∞ is 0.822. In order to compare the pressure distribution of the unsteady computation, Fourier transformation is used here for the pressure distribution. The first mode of the normalized pressure distribution at six span positions are shown in Figs. 4 and 5, where b is the half span. Similar to the results of steady computations, the Euler solver over-predicts the shock wave strength. The position of shock wave from the Euler solver is behind that of the experimental result by about 10 percent of the chord. The Euler computation with the boundary layer correction notably improves. In the outer region, the positions and strengths of the shock waves predicted by the coupled Euler and boundary-layer method are even better than those by the Navier-Stokes solver.

C. Isogai Wing Aeroelastic Computation

We use the current unsteady coupled Euler and boundary-layer solver in a coupled CFD-CSD method[18] for the two-dimensional Isogai wing model,[19,20] Case A. This model simulates the bending and torsional motion of a wing cross-section in the outboard portion of a swept wing. It consists of two degrees of freedom, plunging and pitching, for a NACA 64A010 airfoil. We compute the case with the current coupled method and compare the results of the Euler equations in Ref. 18. The details of the structural model can be found in Ref. 21 as well as in Refs. 19 and 20. The case whose mass ratio μ= 60 is considered. The Reynolds number is 6×10^6.

In order to compute the flutter boundary, different values of speed index V$_f$ are tested. V$_f$ is defined as

$$V_f = \frac{2U_\infty}{c\omega\sqrt{\mu}} \tag{24}$$

where ω is the lowest natural frequency of the structure, μ is the mass ratio. In order to compare the effect of boundary-layer correction, both the Euler solver and the coupled Euler and boundary-layer solver are used to compute the flutter boundary. The computational results are shown in Fig. 6. The flutter boundary from the Euler solver with boundary-layer correction is compared with that by the Euler equations alone and that by the Navier-Stokes solver from Prananta, Hounjet, and Zwann.[22] The transonic "dip" are predicted by both inviscid and viscous solutions. The Euler solution with boundary-layer correction approaches the results of the Navier-Stokes solution. The "S"-shape predicted by the Euler solver vanishes when the viscous effect is taken into account. In order to compare the differences in detail, two typical cases are tested by the Euler and the Euler with boundary-layer correction solvers, respectively. The Mach number M_∞ is 0.875. The first case is with speed index V_f=1.00. The computational results are shown in Fig. 7. With the same initial disturbance, the result with the Euler solver is shown in (b). The amplitudes of pitching and plunging keep increasing until reaching a limited cycle oscillation (LCO) condition. The LCO condition indicates the system is unstable. The solution from the Euler equations with boundary-layer correction is shown in (a), which shows that the amplitudes of pitching and plunging keep decreasing, indicating that the system is stable. At V_f=2.30, the situation is opposite to previous case. The comparison is shown in Fig. 8. The Euler solution is stable, but the result by coupled Euler and boundary-layer method is unstable.

VII. Summary and Conclusion

An interactive boundary-layer method is presented for time-domain aeroelastic computation. The method solves the three-dimensional unsteady Euler equations and Green's lag entrainment integral boundary-layer equations. The Euler equations are solved on stationary body-fitted curvilinear grids. Unsteady boundary conditions on moving surfaces are approximated by a small-perturbation method based on Taylor expansions around the non-moving mean position of the surfaces. This eliminates the need of moving grid. A "semi-inverse" method is used to couple the Euler and the integral boundary solutions in order to handle flow with strong inviscid and viscous interactions. Comparisons of the solutions by the interactive boundary-layer method for steady and unsteady transonic flows with those by the Navier-Stokes equations and available experimental data show significant improvement by the present method over the solutions by the Euler equations alone. The method is used to predict the flutter boundary of the Isogai wing model. The solutions by the interactive boundary-layer method agree with those by a Navier-Stokes method and demonstrate a substantial difference between the flutter behaviors predicted by viscous and inviscid methods in the transonic

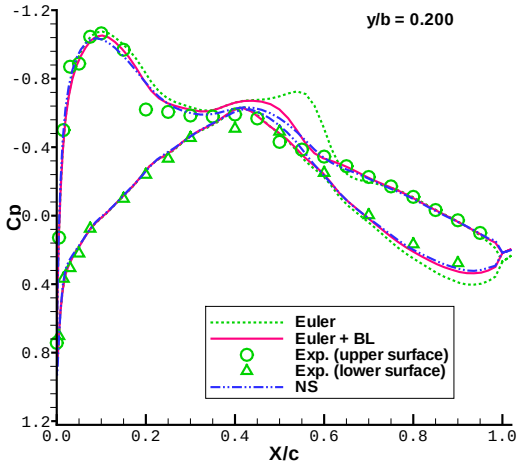

(a) y/b=0.200

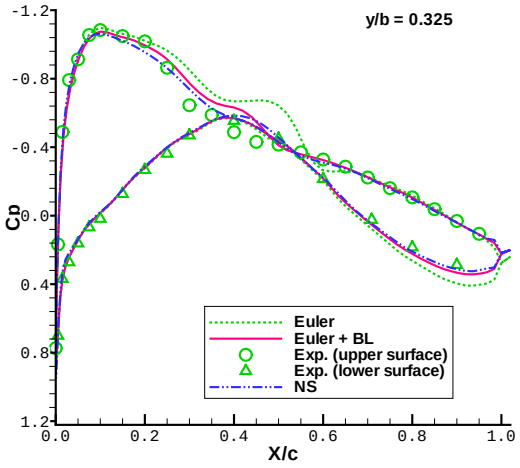

(b) y/b=0.325

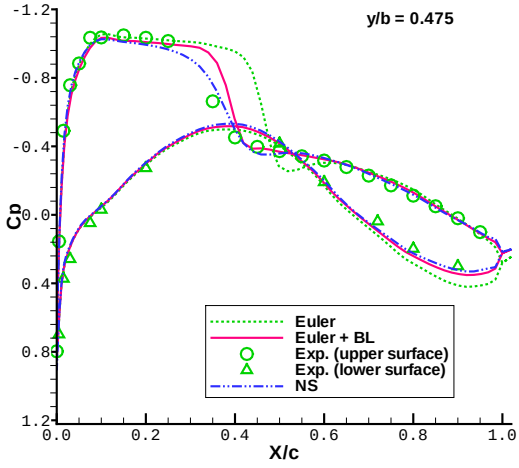

(c) y/b=0.475

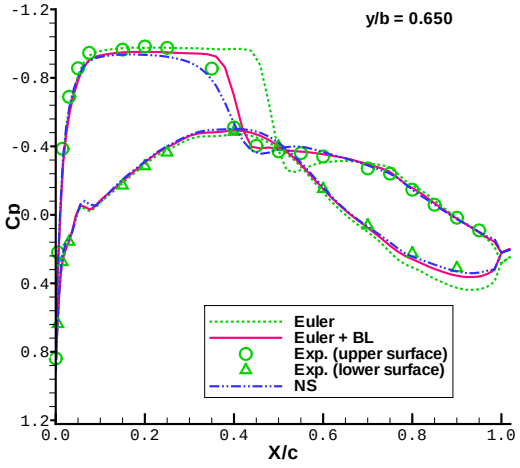

(d) y/b=0.650

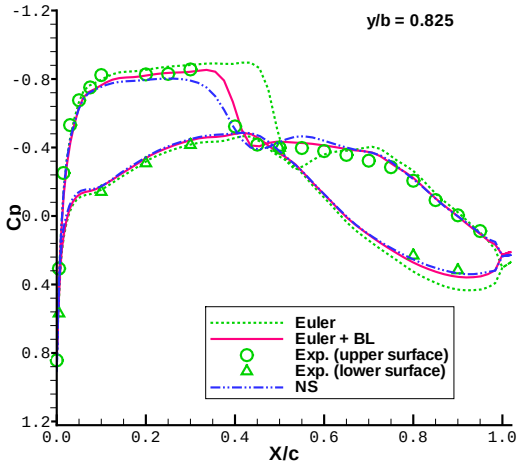

(e) y/b=0.825

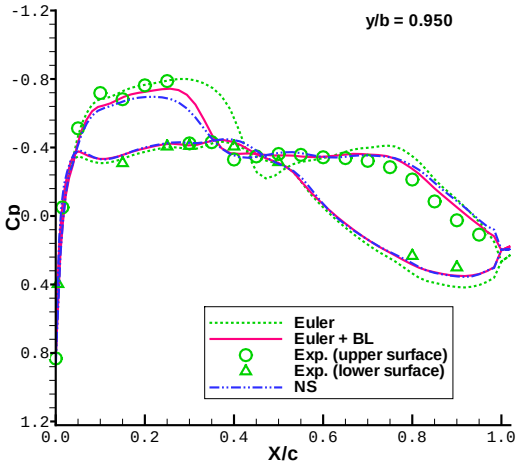

(f) y/b=0.950

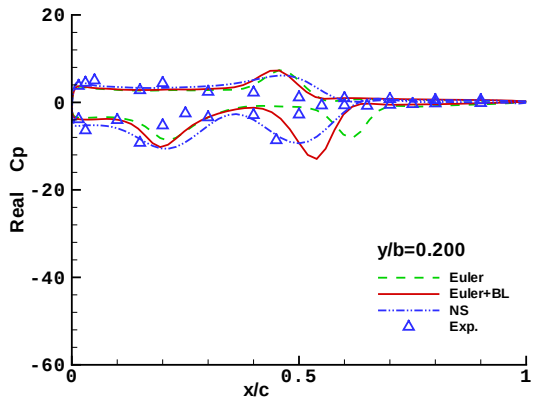

(a) y/b=0.200

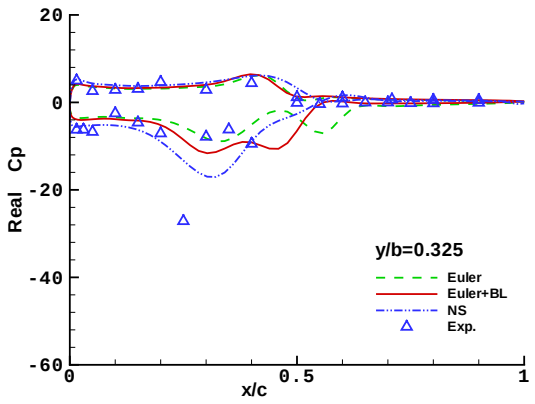

(b) y/b=0.325

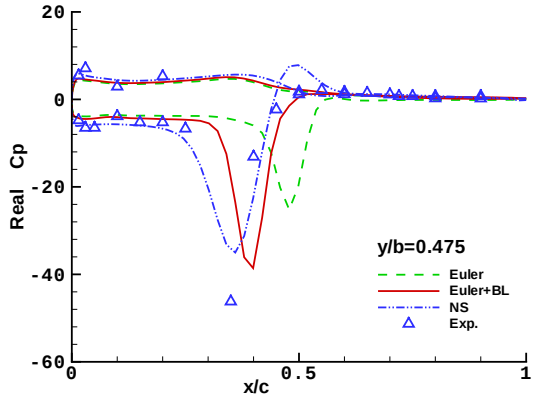

(c) y/b=0.475

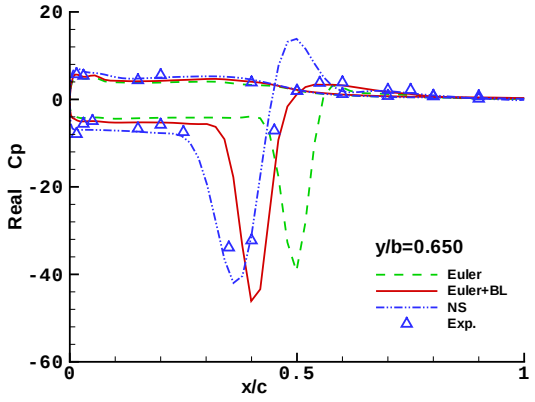

(d) y/b=0.650

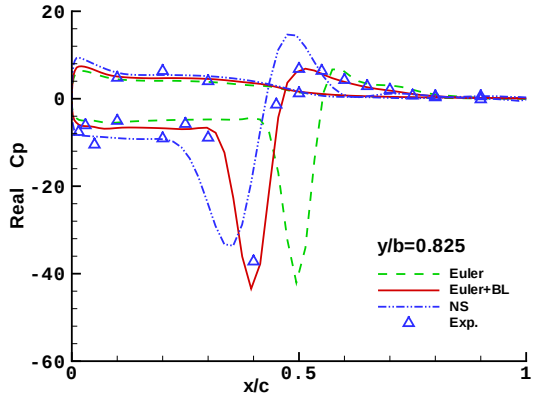

(e) y/b=0.825

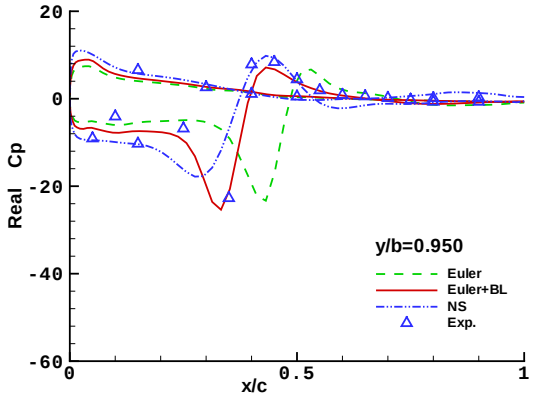

(f) y/b=0.950

Figure 4. Comparison of unsteady pressure distribution for LANN Wing $M_\infty = 0.822$ $\alpha_0 = 0.60°$, $\alpha_m = 0.50°$, κ=0.102 (Real part)

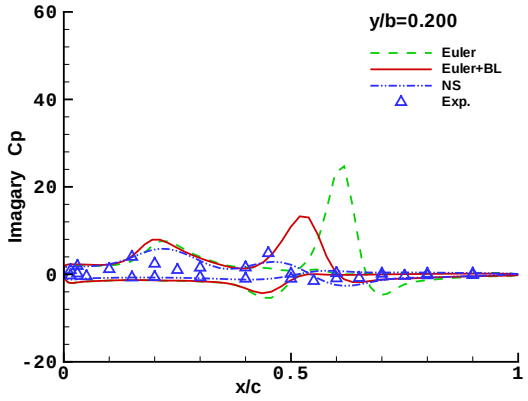

(a) y/b=0.200

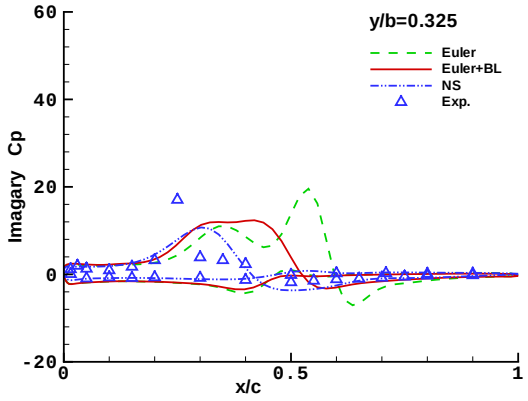

(b) y/b=0.325

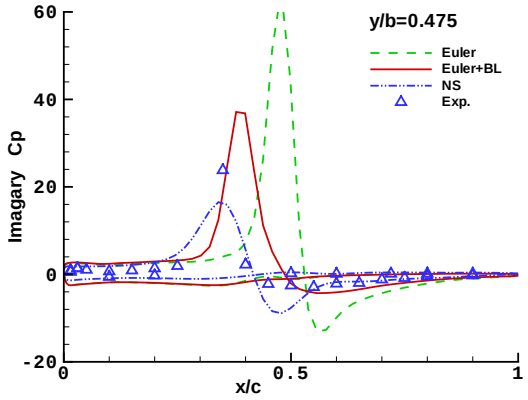

(c) y/b=0.475

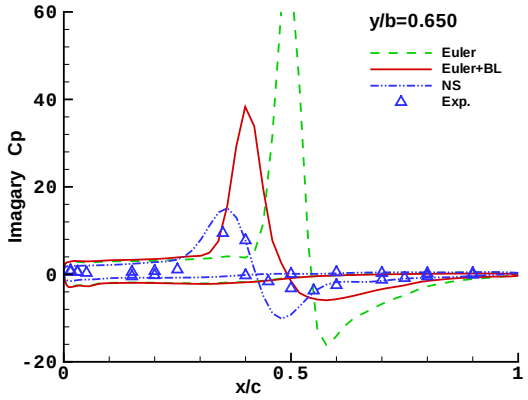

(d) y/b=0.650

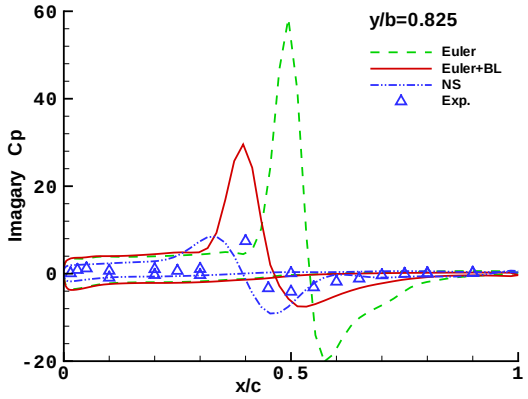

(e) y/b=0.825

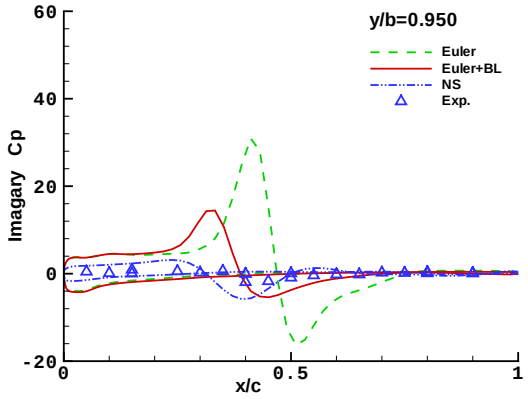

(f) y/b=0.950

Figure 5. Comparison of unsteady pressure distribution for LANN Wing $M_\infty = 0.822$ α_0 = 0.60°, α_m = 0.50°, κ=0.102 (Imaginery part)

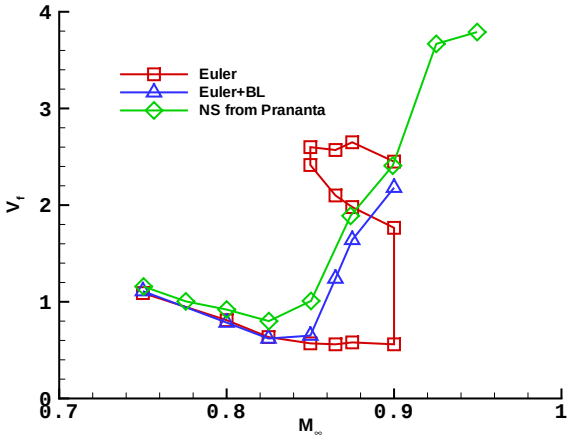

Figure 6. Comparison of flutter boundary of Isogai wing.

range. Previous results by the Euler equations show dual flutter points for a given Mach number, which results in an S-shaped flutter boundary in the $V_f - M_\infty$ plane. This multiplicity of flutter points are not present in the viscous predictions. The computations demonstrate that the present interactive boundary-layer method is a convenient and efficient alternative in place of a full unsteady Reynolds-Averaged-Navier-Stokes solver for aeroelastic simulations.

References

[1]Shuster, D. M., Liu, D., and Huttsell, L. J., "Computational Aeroealsticity: Success, Progress, Challenge," *Journal of Aircraft*, Vol. 40, No. 5, Sept. 2003, pp. 843–856.

[2]Zhang, Z., Liu, F., and Shuster, D. M., "Calculation of unsteady shock boundary-layer interaction by an Euler method coupled with an integral boundary-layer method on Cartesian grids," AIAA Paper 2004-5203, Aug. 2004.

[3]Sadeghi, M., Yang, S., and Liu, F., "Parallel Computation of Wing Flutter with a Coupled Navier-Stokes/CSD Method," AIAA Paper 2003-1347, Jan. 2003.

[4]Yang, S., Luo, S., Liu, F., Tsai, H.-M., and Shuster, D. M., "Time-Domain Aeroelastic Simulation on Stationary Body-Conforming Grids with Small Perturbation Boundary Conditions," AIAA Paper 2004-0885, Jan. 2004.

[5]Yang, S., Liu, F., Luo, S., Tsai, H.-M., and Shuster, D. M., "Three-Dimensional Aeroelastic Computation Based on Stationary Body-Conforming Grids with Small Perturbation Boundary Conditions," AIAA Paper 2004-2235, June 2004.

[6]Liu, F. and Jameson, A., "Multigrid Navier-Stokes Calculations for Three-Dimensional Cascades," *AIAA Journal*, Vol. 31, No. 10, October 1993, pp. 1785–1791.

[7]Liu, F. and Ji, S., "Unsteady flow calculations with a multigrid Navier-Stokes method," *AIAA Paper 95-2205*, June 1995.

[8]Vatsa, V. and Carter, J., "Development of an Integral Boundary-Layer Technique for Separated Turbulent Flow," United Technologies Research Center Report UTRC81-28, June 1981.

[9]Head, M., "Entrainment in the turbulent boundary layer," A.R.C.R.&M. 3152, 1958.

[10]Green, J. E., Weeks, D. J., and Brooman, J. W. F., "Prediction of Turbulent Boundary Layers and Wakes in Compressible Flow by a Lag-Entrainment Method," British Aeronautical Research Council R & M 3791, 1977.

[11]Thwaites, B., "Approximate Calculation of the Laminar Boundary Layer," *Aeronaut. Q.*, Vol. 1, No. 6, 1949, pp. 245–280.

[12]Michel, R., "Etude de la Transition sur les Profiles d'Aile," ONERA Report 1/1578A, 1951.

[13]Carter, J. E., "A New Boundary-Layer Inviscid Iteration Technique for Separated Flow," AIAA Paper 1979-1450, July 1979.

[14]Sockol, P. M. and Johnston, W. A., "Coupling Conditions for Integrating Boundary Layer and Rotational Inviscid Flow," *AIAA Journal*, Vol. 24, No. 6, June 1986, pp. 1033–1035.

[15]McCroskey, W. J., "A critical assessment of wind tunnel resutls for the NACA 0012 airfoil," AGARD CP 429, Paper No. 1, 1987.

[16]Cook, P. H., Mcdonald, M. A., and Firmin, M. C. P., "Airfoil RAE 2822 - Pressure distribution and boundary layer and wake measurements," AGARD AR 138, 1979.

[17]Zwaan, R., "LANN Wing pitching oscillation," Compendium of Unsteady Aerodynamics Measurements, AGARD Report 702 Addendum, 1985.

[18]Liu, F., Cai, J., Zhu, Y., Wong, A. S. F., and Tsai, H.-M., "Calculation of Wing Flutter by a Coupled Fluid-Structure Method," *Journal of Aircraft*, Vol. 38, No. 2, Mar.-Apr. 2001, pp. 334–342.

[19]Isogai, K., "On the Transonic-Dip Mechanism of flutter of a Sweptback Wing," *AIAA Journal*, Vol. 17, No. 7, July 1979, pp. 793–795.

[20]Isogai, K., "On the Transonic-Dip Mechanism of flutter of a Sweptback Wing: Part II," *AIAA Journal*, Vol. 19, No. 9, Sept. 1981, pp. 1240–1242.

[21]Alonso, J. J. and Jameson, A., "Fully-Implicit Time-Marching Aeroelastic Solutions," AIAA Paper 94–0056, Jan. 1994.

[22]Prananta, B. B., Hounjet, M. H. L., and Zwann, R. J., "Two-dimensional transonic aeroelastic analysis using thin layer Navier-Stokes methods," *J. of Fluid and Structure*, Vol. 12, 1998, pp. 655–676.

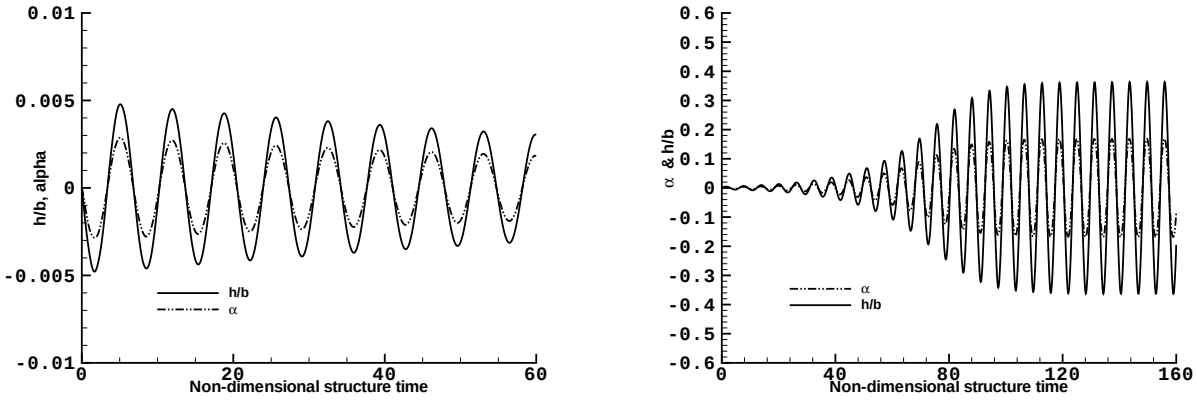

(a) Euler+BL (b) Euler

Figure 7. Time history of pitching and plunging motion for Isogai wing model for $M_\infty = 0.8750$ $\mathbf{V}_f = \mathbf{1.00}$.

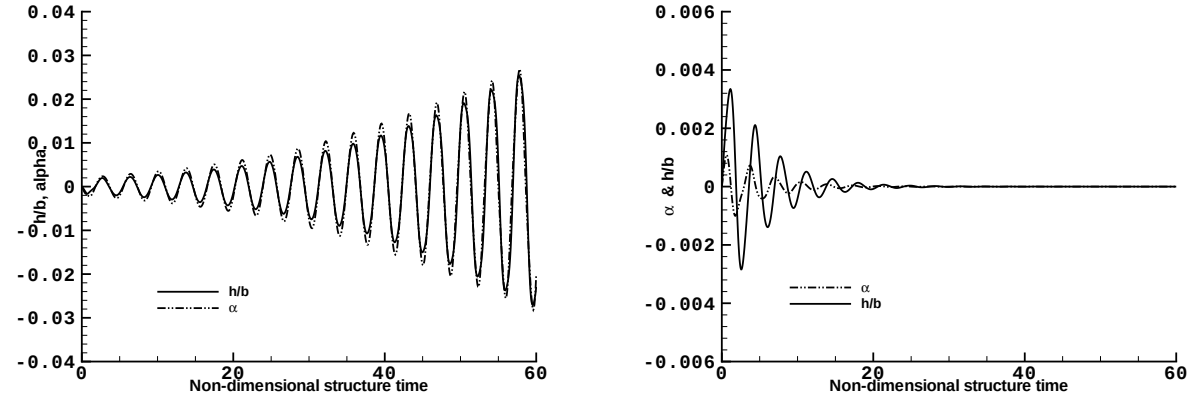

(a) Euler+BL (b) Euler

Figure 8. Time history of pitching and plunging motion for Isogai wing model for $M_\infty = 0.875$ $\mathbf{V}_f = \mathbf{2.30}$.